Editors' Suggestion

Exact Matrix Product States at the Quantum Lifshitz Tricritical Point in a Spin-1/2 Zigzag-Chain Antiferromagnet with Anisotropic Γ Term

Hidehiro Saito* and Chisa Hotta†
Department of Basic Science, University of Tokyo, Meguro-ku, Tokyo 153-8902, Japan

(Received 29 November 2023; revised 31 January 2024; accepted 27 March 2024; published 16 April 2024)

Quantum anisotropic exchange interactions in magnets can induce competitions between phases in a different manner from those typically driven by geometrically frustrated interactions. We study a one-dimensional spin-1/2 zigzag chain with such an interaction, Γ term, in conjunction with the Heisenberg interactions. We find a ground state phase diagram featuring a multicritical point where five phases converge: a uniform ferromagnet, two antiferromagnets, Tomonaga-Luttinger liquid, and a dimer-singlet coexisting with nematic order. This multicritical point is simultaneously quantum tricritical and Lifshitz, and most remarkably, it hosts multidegenerate ground state wave functions with the degeneracy increasing in squares of system size. The exact ground states are obtained in the matrix product form opening wide applications to frustration-free models.

DOI: 10.1103/PhysRevLett.132.166701

Introduction.—Traditionally, phase diagrams for quantum magnetism in one dimension (1D) are quite simple, predominantly characterized by the Tomonaga-Luttinger liquid (TLL) which sometimes undergoes a transition to a magnetic phase breaking discrete symmetries like Ising Néel order. The introduction of geometrical frustrations can lead to emergent quantum disordered phases such as dimer-singlet phase on a zigzag chain [1–6] and the nematic phase on frustrated ladders [7,8]. These states are sufficiently trivial in the context of quantum topology, as they are approximated by product-state wave functions. Still, a realization of the Majumdar-Ghosh (MG) state [1,2] inside the dimer-singlet phase may deserve particular emphasis, because it stands as one of a handful of exact ground states in realistic quantum many-body models.

Recently, quantum anisotropic exchange interactions have been added as another ingredient to enrich quantum magnetism. An iconic example is the Kitaev interaction that serves as a source of spin liquid with long-range entanglement and topological excitations [9–11]. In reality, the Kitaev interaction cannot avoid coexistence with the Γ and Heisenberg terms that largely restrict the phase space of spin liquid [12,13]. However, a very rich phase diagram with spiral, stripe, or other spatially modulated phases [14] show that they provide strong frustration or competition in a way not easily attained by the geometrical frustration effect.

The anisotropic exchange interactions can naturally arise in the Mott insulating state of 4d, 5d, and 4f electrons with strong spin-orbit couplings like iridium oxides, iridates, and rare-earth magnets [15,16]. When derived microscopically, they are classified into three categories; Kitaev-type bond-oriented diagonal exchange, Γ term representing bond-symmetric, off-diagonal (different spin component) exchange, and the bond-antisymmetric Dzyaloshinskii-Moriya exchange interactions. For rare-earth-based materials with high crystal symmetric octahedral ligands, the SU(2) symmetric Heisenberg interactions are dominant and a small Γ term adds on top of that [17,18]. In this Letter, we clarify the role of the Γ term by simplifying it to an idealized form in a 1D zigzag Heisenberg chain with geometrical frustration. Although the Γ term was previously a less important secondary term in the Kitaev magnetism, our ground state phase diagram turns out to be rich, as it includes the multicritical point showing both the Lifshitz and tricritical nature [19–23].

The Lifshitz point is a finely adjusted point in a phase diagram at which a uniform phase and a spatially modulated ordered phase meet the disordered phase [20,24]. In the early days, it was discussed in the ANNNI model [25]. Similarly, the multicritical point in metamagnets is explained by the competing antiferromagnetic and spin flopped states in a magnetic field [21,26–28] or in liquid ^{4}He [29]. These examples are governed by two competing Ising order parameters that originate from the explicit magnetic anisotropies of the Hamiltonian. By contrast, in our case, the compatibility of the Γ term and the discrete symmetry of the crystal lattice spontaneously select the magnetic easy axis, generating three Ising order parameters. The three are decoupled in the Landau theory and will form a Gaussian fixed point similar to the bicritical or tetracritical point of the metamagnets [26,27]. Our tricritical Lifshitz point stands out because it occurs at zero temperature and meets the quantum disordered phase. It falls exactly on the MG line with exact singlet states, and most intriguingly, its multidegenerate ground states turn out

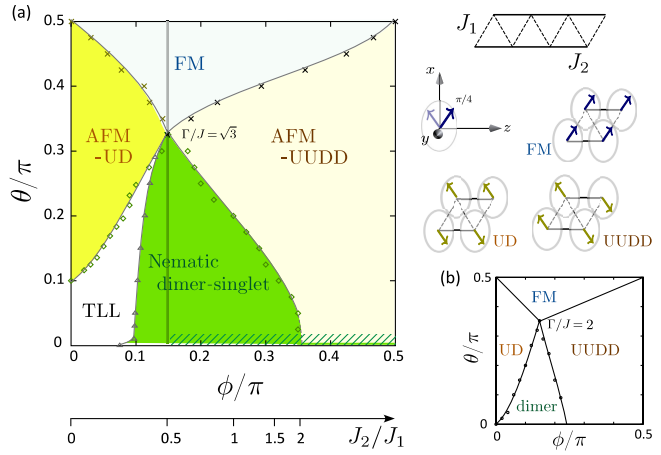

FIG. 1. (a) Ground state phase diagram of Eq. (1) obtained by DMRG. Solid line $J_2/J_1 = 1/2 = \arctan(\phi)$ is the Majumdar-Ghosh line where the singlet product state is the exact eigenstate. The multicritical point is located on that line at $\Gamma_\eta/J_\eta = \sqrt{3}$. The right panels show the zigzag chain and the global xyz coordinate, where UD and UUDD have (1,1,0) and the Ferro phase has $(1,-1,0)$ as a spontaneously emergent easy axis of magnetic moment, respectively. (b) Mean-field phase diagram where the multicritical point appears at $(\Gamma_\eta/J_\eta, J_2/J_1) = (2, 1/2)$. The data points are the mean-field solution from the bond operator approach based on the dimer.

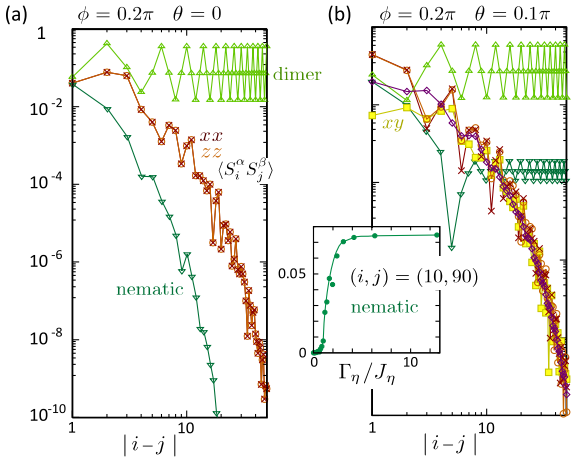

FIG. 2. (a) Two-point correlation functions $\langle O_i O_j \rangle$ of spins $O_i = S_i^{\alpha_i}$ of $(\alpha_i \alpha_j) = xx, zz$, and xy; dimer $O_i = \boldsymbol{S}_i \cdot \boldsymbol{S}_{i+1}$; and nematic operators $O_i = S_i^x S_{i+1}^y + S_i^y S_{i+1}^x$ obtained by DMRG with $N = 100$. (a) $\theta = 0$ and (b) $\theta = 0.1\pi$ with $\phi = 0.2\pi$. Inset shows the evolution of nematic correlation at $(i, j) = (10, 90)$ with Γ_η/J_η.

to be exactly described by a matrix product state (MPS) representation.

Model and phase diagram.—We consider a quantum spin-1/2 Hamiltonian on a zigzag chain given as

$$\mathcal{H} = \sum_j \sum_{\eta=1,2} J_\eta \boldsymbol{S}_j \cdot \boldsymbol{S}_{j+\eta} + \Gamma_\eta (S_j^x S_{j+\eta}^y + S_j^y S_{j+\eta}^x), \quad (1)$$

where J_η and Γ_η are the Heisenberg and anisotropic exchange interactions between nearest ($\eta = 1$) and next nearest ($\eta = 2$) spins for which we take site indices alternatively between legs. For later convenience, we parametrize them as $\Gamma_1/J_1 = \Gamma_2/J_2 = \tan\theta$ and $J_2/J_1 = \Gamma_2/\Gamma_1 = \tan\phi$, where the range $0 \le \phi$, $\theta \le \pi/2$ corresponds to antiferromagnetic J_1 and J_2 [30–32]. The sign of Γ_η does not matter as it is erased by the local unitary transformation. We take the spin quantization axis as the one shown in Fig. 1; the z axis is taken parallel to the chain and we set the y axis perpendicular to the triangular plane.

We show in Fig. 1(a) the ground state phase diagram of Eq. (1) obtained by the density matrix renormalization group (DMRG) calculation [33]. Here, we take typically $N = 100$ lattice sites and adopt two cases—open boundary condition (OBC) and a sine-square deformation (SSD)—where the latter can accurately evaluate incommensurate ordering and suppresses finite-size effects [34–36]. The $\Gamma_\eta = 0$ ($\theta = 0$) limit is the zigzag J_1-J_2 model where the transition from a TLL phase to the dimer-singlet phase occurs at $J_2/J_1 \sim 0.241$ [2–6]. At $\Gamma_\eta \neq 0$, the two phases extend and undergo a second order transition to the antiferromagnetically ordered (AFM) phases which we call UD and UUDD for $J_2/J_1 \le 0.5$ and ≥ 0.5, respectively. The AFM phases experience first-order transitions to the ferromagnetic (FM) phase. The magnetic moments of the two AFM phases are locked parallel to $(x, y, z) = (1, 1, 0)$ and that of FM phase to $(1, -1, 0)$. Similar spin orientation is observed in the 1D Heisenberg chain with a bond alternating Γ term [37].

The phase diagram has a few remarkable features. First, the three second-order transition lines separating UD, TLL, dimer-singlet, and UUDD meet at the single point, $(J_2/J_1, \Gamma_\eta/J_\eta) = (1/2, \sqrt{3})$. It is the end point of the two first-order transition lines separating the FM and UD, UUDD phases. This point is tricritical because the three order parameters are adjusted as we see shortly.

Second, we find that $J_2/J_1 = \Gamma_2/\Gamma_1 = 1/2$ is a MG line; the singlet product state, $|\Psi_{\mathrm{MG}}\rangle = \prod_{j=1}^{N/2} |s_j\rangle$ with $|s_j\rangle = (|\uparrow\downarrow\rangle - |\downarrow\uparrow\rangle)/\sqrt{2}$ on $[2j-1, 2j]$ sites continues to be the exact eigenstate of Eq. (1).

Finally, at $\Gamma_\eta \neq 0$ and off the MG line, the nematic order emerges inside the dimer-singlet phase at all finite values of Γ_η [38]. Figure 2 shows two-point correlation functions of magnetic and nonmagnetic operators obtained by DMRG. At $\Gamma_\eta = 0$, all the magnetic correlations decay exponentially with distances, and the singlet-singlet correlation function dominates. When $\Gamma_\eta > 0$, a nematic-nematic correlation starts to sustain at $|i-j| \to \infty$, whose value continuously increases from a zero at $\Gamma_\eta = 0$.

Multicriticality.—We first clarify the underlying competition of phases near the multicritical point. To

illustrate it, we prepare the basis set of site j using the up and down spin states about the global xyz coordinate, $|\uparrow\rangle, |\downarrow\rangle$, as $|u\rangle_j = |\uparrow\rangle_j + e^{i\pi/4}|\downarrow\rangle_j$, $|d\rangle_j = |\uparrow\rangle_j - e^{i\pi/4}|\downarrow\rangle_j$, $|f\rangle_j = |\uparrow\rangle_j + e^{i3\pi/4}|\downarrow\rangle_j$, and its conjugate $|f^*\rangle_j$. Their magnetic moment points in the $(\pm 1, \pm 1, 0)$ direction for $|u\rangle$ and $|d\rangle$, and $(\pm 1, \mp 1, 0)$ for $|f\rangle$. The variational scheme considering a maximally four-site-period naturally provides a product state $\prod_{j=1}^{N} |\psi_j\rangle$ where $|\psi_j\rangle$ is expanded as a linear combination of the above-mentioned four sites. The lowest energy state gives the following mean-field solutions: $|\Psi_{\mathrm{UUDD}}\rangle = \prod_{j=1}^{N/4} |u\rangle_{4j-3}|u\rangle_{4j-2}|d\rangle_{4j-1}|d\rangle_{4j}$, $|\Psi_{\mathrm{UD}}\rangle = \prod_{j=1}^{N/2} |u\rangle_{2j-1}|d\rangle_{2j}$, and $|\Psi_{\mathrm{FM}}\rangle = \prod_{j=1}^{N} |f\rangle_j$, whose energies are $E_{\mathrm{UUDD}} = -(J_2 + \Gamma_2)N/4$, $E_{\mathrm{UD}} = (-J_1 - \Gamma_1 + J_2 + \Gamma_2)N/4$, and $E_{\mathrm{FM}} = (J_1 - \Gamma_1 + J_2 - \Gamma_2)N/4$, respectively. These three states are exclusive to each other and meet at $\Gamma/J = 2$ in the mean-field phase diagram in Fig. 1(b); it is slightly off the exact multicritical point, while successfully capturing the essence of the numerical phase diagram. Here, we have added the data points derived from the bond-operator mean field approach [39,40] based on dimers, which will be discussed elsewhere.

The implications of the mean-field results become distinct when we rotate the spin coordinate by $\pi/4$ about the z axis; The Hamiltonian in the new coordinate $x'y'z'$ is given as $\mathcal{H}^{\pi/4} = \mathcal{H}_{x'y'} + \mathcal{H}_{z'}$, and by dropping off $\mathcal{H}_{z'}$, we obtain $\mathcal{H}^{\pi/4} \sim \mathcal{H}_{x'y'}$ with

$$\mathcal{H}_{x'y'} = \sum_{j=1}^{N} \sum_{\eta=1,2} (J_\eta - \Gamma_\eta) S_j^{x'} S_{j+\eta}^{x'}, + (J_\eta + \Gamma_\eta) S_j^{y'} S_{j+\eta}^{y'}, \tag{2}$$

where $\mathcal{H}_{z'} = \sum_{j=1}^{N} \sum_{\eta=1,2} J_\eta S_j^{z'} S_{j+\eta}^{z'}$ is irrelevant [26]. The U and D in the mean-field solutions are the Ising type solution of Eq. (2) in the y' directions, and FM is the one in the x' direction, whose energies cross at the multicritical point. Indeed, in examining the simplest long wavelength excitations of Eq. (2) from the multidegenerate ground state, the Ising types of a ferromagnetic mode pointing toward x' and the two other magnetic modes in the y' direction are observed (see Supplemental Material [41]).

As another way of understanding this spontaneous selection of magnetic easy axes, one may go back to Eq. (1), finding that it is invariant under the π rotation about both the (1,1,0) and $(-1, 1, 0)$ axes, which transforms the spins as $(S^x, S^y, S^z) \to (S^y, S^x, -S^z)$ and $(-S^y, -S^x, -S^z)$, respectively. These two directions are thus robust against the quantum fluctuation and hence are encoded in Eq. (1) as invisible easy axes.

The two or more competing Ising states remind us of a bicritical or tetracritical point of the ANNNI model [25] and metamagnets [21,26–28]. Their origin, the competing ferromagnetic and antiferromagnetic Ising exchanges in the former, and the magnetic easy axis and the transverse magnetic field in the latter are visible in their Hamiltonian. Their multicritical phase transition at finite temperature occurs due to the thermal entropic effect. In contrast, our Ising anisotropy comes from the interplay of quantum anisotropic exchange and the lattice symmetry, and the quantum disorder due to quantum fluctuation drives the multicriticality at zero temperature.

Exact solutions.—When $J_1 = 2J_2 \equiv 2J$ and $\Gamma_1 = 2\Gamma_2 = 2\Gamma$, the couplings of diagonal rungs are doubled from those of legs, and the Hamiltonian Eq. (1) can be rewritten as the sum of local Hamiltonians, h_l, of the lth triangular unit based on $[l+1, l, l-1]$-th spins as $\mathcal{H} = \sum_l \hat{h}_l$ with

$$\hat{h}_l = \sum_{i,j \in l} J \boldsymbol{S}_i \cdot \boldsymbol{S}_j + \sum_{i,j \in l} \Gamma (S_i^x S_j^y + S_i^y S_j^x), \tag{3}$$

which is shown schematically in Fig. 3(a). At $\Gamma = 0$, the lowest energy of $\hat{h}_l = J(\boldsymbol{S}_{l-1} + \boldsymbol{S}_l + \boldsymbol{S}_{l+1})^2/2 - 9J/8$ is $\epsilon_0 = -3J/4$, attained by a total $S = 1/2$ for all triangle which is the MG state. When $\Gamma > 0$, J and Γ terms in Eq. (3) commute and the MG singlet state remains as the exact eigenstate of Eq. (1), which is equivalent to the MG state known in the XYZ model [42], i.e., $\mathcal{H}^{\pi/4}$. Notice that the J and Γ terms of Eq. (1) *do not commute*.

At the multicritical point, $\Gamma/J = \sqrt{3}$, the ground state is highly degenerate including a doubly degenerate MG state. This is already unusual because conventional critical ground states typically lack such degeneracy. Even more exceptional is that the degrees of degeneracy and *a full set of exact solutions* are accessible. To prove this, we present two methodologies: the first involves solving a set of linear equations satisfying conditions to have the energy $E = -N\epsilon_0$, while the second entails iteratively constructing a matrix product state. In these methods, we employ a triangular open boundary condition (T-OBC) shown in Fig. 3(a); suppose that we have a set of degenerate ground states of $\mathcal{H} = \sum_{l=1}^{N} \hat{h}_l$ under a periodic boundary condition (PBC). Even if we eliminate the two triangles, h_1 and h_N, as illustrated in Fig. 3(a), all the degenerate ground states persist as those of $\mathcal{H} = \sum_{l=2}^{N-1} \hat{h}_l$ with energy $-(N-2)\epsilon_0$.

Solving linear equations.—There are eight eigenstates of a triangular unit in Eq. (3). Using 0/1 representing up or down spins on $[l+1, l, l-1]$ sites in the descending order, they read

$$|\psi_{n\Uparrow}^{\pm}\rangle = \sqrt{3}|000\rangle \pm i(|011\rangle + |101\rangle + |110\rangle), \tag{4}$$

$$|\psi_{m\Downarrow}\rangle = |011\rangle + \omega|101\rangle + \omega^2|110\rangle, \tag{5}$$

with $\omega = e^{i2\pi/3}$, where $\Uparrow$ states are obtained from the $\Downarrow$ ones by converting the spins as $0 \leftrightarrow 1$. Four "nematic" states with $S = 3/2$, $|\psi_{n\Uparrow}^{\pm}\rangle$, $|\psi_{n\Downarrow}^{\mp}\rangle$, have energy $3J/4 \pm \sqrt{3}\Gamma/2$ and four magnetic states, $|\psi_{m\Uparrow}\rangle$, $|\psi_{m\Uparrow}^*\rangle$, $|\psi_{m\Downarrow}\rangle$, $|\psi_{m\Downarrow}^*\rangle$ with

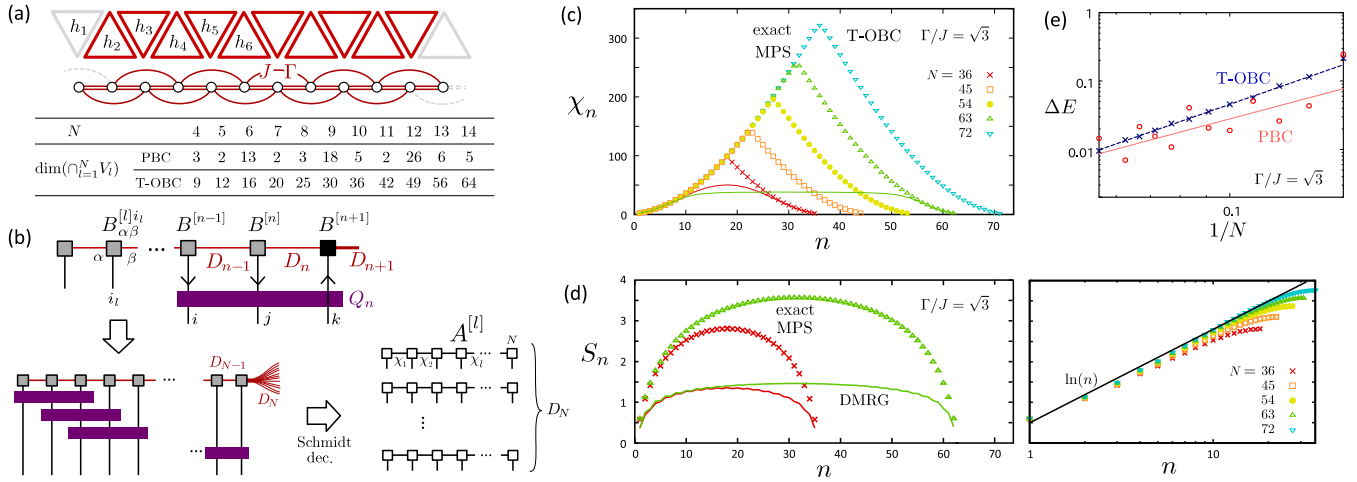

FIG. 3. (a) Illustration of the model at $J_1 = 2J_2 = 2J$, $\Gamma_1 = 2\Gamma_2 = 2\Gamma$ as a sum of h_l with $l = 2, \ldots, N-1$ (T-OBC), in comparison with the 1D description, and the degeneracy of the ground state D_N up to $N = 14$ for PBC and T-OBC. (b) Protocol to construct an exact MPS with T-OBC. Matrix $B^{[n+1]}$ is successively generated from the nth and $(n-1)$-th matrix elements by solving linear equations represented by Q_n. The matrix elements of $B^{[l]}$ $(l = 1, \ldots, N)$ are separated into a set of D_N independent degenerate MPS $\{A^{[l]}\}$. (c) Bond dimensions χ_n of exact MPS $A^{[l]}$ for $N = 36, 45, 54, 63, 72$. (d) Entanglement entropy S_n of the exact MPS with $N = 36, 63$ and T-OBC about the bipartition to n and $(N-n)$-site subsystems as a function of n. Data are averaged over complete orthogonal degenerate ground states (Supplemental Material C [41]). Right panel gives the entanglement scaling: Solid line is $S_n \sim (c/3)\ln n$ with $c = 3$. Solid lines in panels (c) and (d) are the corresponding DMRG results with numerically accurate energy Ne_0. (e) Energy gap ΔE between the ground state Ne_0 and the first excited state obtained by ED for T-OBC and PBC. Solid-broken line shows the guide for finite-size scaling behavior $\Delta E \propto N^{-2}$ (PBC) and $N^{-2.60}$ (T-OBC).

$S = 1/2$ have energy $-3J/4$ along the MG line. Among them, six are the constituents of the ground state at $\Gamma = \sqrt{3}J$, $\{|\psi_l^{\rm gs}\rangle\} \equiv \{|\psi^-_{n\Uparrow}\rangle, |\psi^+_{n\Downarrow}\rangle, |\psi_{m\Uparrow}\rangle, |\psi^*_{m\Uparrow}\rangle, |\psi_{m\Downarrow}\rangle, |\psi^*_{m\Downarrow}\rangle\}$. Because triangles share edges, the entire ground states need to entangle these six bases in a nontrivial manner. Most straightforwardly, we can project out the two excited states on each triangle. Let the subspace of the Hilbert space be given as $V_l = \{\{|\psi_l^{\rm gs}\rangle\} \otimes |j\rangle_{j=1,\ldots,2^{N-3}}\}$, where $\{|j\rangle\}$ is the subspace spanned by the $N-3$ sites that do not belong to the lth triangle. All the states on $\cap_{l=1}^{N} V_l$ are the ground state $|\Psi\rangle$; they satisfy two conditions per triangle as $Q|\Psi\rangle = 0$ with

$$Q = \oplus_{l=1}^{N} Q_l, \quad Q_l = \begin{pmatrix} \sqrt{3} & 0 & 0 & -i & 0 & -i & -i & 0 \\ 0 & i & i & 0 & i & 0 & 0 & \sqrt{3} \end{pmatrix}, \quad (6)$$

where the $(i = 1, \ldots, 2^3)$-th columns of Q_l operate on the states of the lth triangle in the bit representation of i, namely, $|000\rangle, |001\rangle, \ldots, |111\rangle$, we applied in Eq. (5). The number of linear equations is $(N-2) \times 2^{N-2}$. We numerically confirmed that solving them gives a full set of ground states by comparing with the full exact diagonalization (ED) of the original Hamiltonian, while the practically available size is limited to $N \lesssim 20$. However, the number of degeneracy of the ground states is $D_N = \dim(\cap_{l=1}^{N} V_l) = 2^N - \mathrm{rank}Q$, which is obtained iteratively by $\dim(\cap_{i=1}^{n} V_i)/\dim(\cap_{i=1}^{n-1} V_i) = [(n+4)/2(n+2)]$ (even n) and $[(n+5)/2(n+3)]$ (odd n) and we find,

$$D_N = \begin{cases} (N+2)^2/4 & (\text{even } N) \\ (N+1)(N+3)/4 & (\text{odd } N). \end{cases} \quad (7)$$

The actual values of D_N are presented in Fig. 3(a).

Exact MPS solutions.—Using MPS [43] is practically important for accurately representing quantum states with large N [44]. Usually, the MPS of the critical state is only approximately available, whereas ours provides a full set and the exact description, and can be generally applied to other frustration-free models [45–47] (for details see Supplemental Material B [41]). The protocol to obtain the MPS is shown schematically in Fig. 3(b). Suppose that we have an n set of matrices that starts from the left edge matrix as $B^{[l]} = B^{[l]i_l}_{\alpha\beta}$ with $l = 1, \ldots, n$; the lth matrix has dimension $D_{l-1} \times D_l \times 2$ with $i_l = 0/1$ spin degrees of freedom. For small n, we can obtain $\{B^{[l]}\}$ by a Schmidt decomposition of the exact wave function of ED. In increasing sites from n to $n+1$, we consider a vector $\boldsymbol{v}$ whose $m = i + 2j + 4k$ element is $(B^{[n-1]i}B^{[n]j}B^{[n+1]k})$, that includes $2D_n$ unknowns of β_{n+1}-th column of $B^{[n+1]k}$. We have D_{n-2} such vector for each choice of the row of $B^{[n-1]i}$. Therefore, $\boldsymbol{v}$ needs to fulfill $2D_{n-2}$ different pairs of linear equations $Q_n\boldsymbol{v} = 0$ using Eq. (6). Solving $2D_{n-2}$ simultaneous equations, we are able to construct at most $2D_n$ different solutions for $2D_n$ unknowns, which altogether form $B^{[n+1]k}$. At $n = N$, we are left with D_N free bonds on the rhs. By separating them into connected elements, we obtain D_N different MPSs; We

left-normalize each MPS to make them orthogonal with each other, and perform a Schmidt decomposition to reduce the bond dimension to discard the zero-weight ones. The final form $\{A^{[n]}\}_{n=1}^{N}$ of $\chi_{n-1} \times \chi_n \times 2$, serves as a full set of ground states. These operations are done by implementing the routines of iTensor [48].

Figure 3(c) shows the bond dimension χ_N of $\{A^{[n]}\}_{n=1}^{N}$ for choices of N with T-OBC. The $n \leq N/2$ ones follow the exact values for all choices of N and are symmetric about the center. The entanglement entropy (EE) S_n about the bipartition to n and $N-n$ obtained by averaging over D_N ground states is shown in Fig. 3(d). They apparently extrapolate to $S_n \sim \log n$. The natural interpretation is that the three exclusive lowest energy modes at the multicritical point (see Supplemental Material [41]) give the three bosonic excitations, and yield $S_n = c\log(n)/3$ [49,50] with central charge $c = 3$ similarly to spin Bose metal [51], although there can be other possibilities. In parallel, we performed the DMRG calculation for T-OBC and compared it with the exact MPS. Because DMRG can only capture one of the degenerate ground states and favor minimally entangled states, the product MG state likely dominates over others, resulting in a plateau of χ_n and much smaller EE. Our exact MPS does not lose any essential information and has an advantage over it.

We finally show in Fig. 3(e) that the excitation energy ΔE above the ground state obtained by ED vanishes at $N \to \infty$ in power of $1/N$, with $z \sim 2$ for PBC, consistent with the long wavelength bosonic excitations, confirming the gapless nature of the multicritical point.

Conclusions.—We discovered a Lifshitz tricritical point in a ground state phase diagram of the spin-1/2 zigzag ladder, and its exact MPS representation in a system of substantially large size N. Over the last fifty years, multicritical points have been revisited several times. Recent ones are reported in materials. In $NbFe_2$, there exists a competition between ferromagnet and spin-density waves, and a magnetic field drives the transition down to low temperature toward the tricritical point [52]. In Cu_2OSeO_3 that hosts skyrmions, magnetic phases compete and exhibit both the tricritical point and the Lifshitz point separately in the magnetic phase diagram [23]. Our case adds an anomalous simultaneous multicritical and Lifshitz point, where five phases meet and have intriguing multidegeneracy. Our study is motivated by a 4f magnet of spin-1/2 zigzag chain, $YbCuS_2$ [18,53–55]. The neutron diffraction measurement reports an incommensurate magnetic structure at $T < T_O \sim 1$ K and a NMR suggests a gapless nonmagnetic excitation. Still, their $\Gamma/J < 0.1$ remains too small to reach a multicritical point in a laboratory.

From the theory point of view, there had been only a few examples of exact MPS states, e.g., AKLT [43,44,56], W state [57,58], Greengerger-Horne-Zeilinger state [59,60], Motzkin chain [45,61], Fredkin model [46,62], and PXP like model for quantum scars [47,63]. These models were so far often artificial or mostly too idealized for quantum computation. The present multicritical MPS adds a rich and useful playground in a physically meaningful model in condensed matter, as its construction is systematically applied to a wide family of frustration-free models.

We thank Tomotoshi Nishino, Frank Pollmann, Shunsuke Furuya, Hosho Katsura, Atsushi Iwaki, and Karlo Penc for discussion, and Takahiro Onimaru, Chikako Moriyoshi, Kenji Ishida, Shunsaku Kitagawa, and Fumiya Hori for communications. This work is supported by the "The Natural Laws of Extreme Universe" (No. JP21H05191) KAKENHI for Transformative Areas from JSPS of Japan, and JSPS KAKENHI Grants No. JP21K03440.

*saito-hidehiro722@g.ecc.u-tokyo.ac.jp
†chisa@phys.c.u-tokyo.ac.jp

[1] C. K. Majumdar and D. K. Ghosh, J. Math. Phys. (N.Y.) **10**, 1388 (1969).
[2] C. K. Majumdar and D. K. Ghosh, J. Math. Phys. (N.Y.) **10**, 1399 (1969).
[3] F. D. M. Haldane, Phys. Rev. B **25**, 4925 (1982).
[4] K. Okamoto and K. Nomura, Phys. Lett. A **169**, 433 (1992).
[5] S. Eggert, Phys. Rev. B **54**, R9612 (1996).
[6] S. R. White and I. Affleck, Phys. Rev. B **54**, 9862 (1996).
[7] T. Hikihara, L. Kecke, T. Momoi, and A. Furusaki, Phys. Rev. B **78**, 144404 (2008).
[8] J. Sudan, A. Lüscher, and A. M. Läuchli, Phys. Rev. B **80**, 140402(R) (2009).
[9] A. Kitaev, Ann. Phys. (Amsterdam) **321**, 2 (2006).
[10] J. Nasu, M. Udagawa, and Y. Motome, Phys. Rev. B **92**, 115122 (2015).
[11] Y. Kasahara, T. Ohnishi, Y. Mizukami, O. Tanaka, S. Ma, K. Sugii, N. Kurita, H. Tanaka, J. Nasu, Y. Motome, T. Shibauchi, and Y. Matsuda, Nature (London) **559**, 227 (2018).
[12] G. Jackeli and G. Khaliullin, Phys. Rev. Lett. **102**, 017205 (2009).
[13] J. Chaloupka, G. Jackeli, and G. Khaliullin, Phys. Rev. Lett. **105**, 027204 (2010).
[14] J. G. Rau, E. K.-H. Lee, and H.-Y. Kee, Phys. Rev. Lett. **112**, 077204 (2014).
[15] W. Witczak-Krempa, G. Chen, Y. B. Kim, and L. Balents, Annu. Rev. Condens. Matter Phys. **5**, 57 (2014).
[16] J. G. Rau, E. K.-H. Lee, and H.-Y. Kee, Annu. Rev. Condens. Matter Phys. **7**, 195 (2016).
[17] J. G. Rau and M. J. P. Gingras, Phys. Rev. B **98**, 054408 (2018).
[18] H. Saito, H. Nakai, and C. Hotta, J. Phys. Soc. Jpn. **93**, 034701 (2024).
[19] E. M. Lifshitz, J. Phys. (Moscow) **6**, 61 (1942).
[20] R. M. Hornreich, M. Luban, and S. Shtrikman, Phys. Rev. Lett. **35**, 1678 (1975).
[21] D. R. Nelson and M. E. Fisher, Phys. Rev. B **11**, 1030 (1975).
[22] A. Abdel-Hady and R. Folk, Phys. Rev. B **54**, 3851 (1996).

[23] H. C. Chauhan, B. Kumar, J. K. Tiwari, and S. Ghosh, Phys. Rev. B **100**, 165143 (2019).
[24] A. Michelson, Phys. Rev. B **16**, 577 (1977).
[25] W. Selke, Phys. Rep. **170**, 213 (1988).
[26] D. R. Nelson, J. M. Kosterlitz, and M. E. Fisher, Phys. Rev. Lett. **33**, 813 (1974).
[27] M. E. Fisher and D. R. Nelson, Phys. Rev. Lett. **32**, 1350 (1974).
[28] J. M. Kosterlitz, D. R. Nelson, and M. E. Fisher, Phys. Rev. B **13**, 412 (1976).
[29] K.-S. Liu and M. E. Fisher, J. Low Temp. Phys. **10**, 655 (1973).
[30] K. Okunishi and T. Tonegawa, J. Phys. Soc. Jpn. **72**, 479 (2003).
[31] K. Okunishi, J. Phys. Soc. Jpn. **77**, 114004 (2008).
[32] T. Hikihara, T. Momoi, A. Furusaki, and H. Kawamura, Phys. Rev. B **81**, 224433 (2010).
[33] S. R. White, Phys. Rev. Lett. **69**, 2863 (1992).
[34] A. Gendiar, M. Daniška, Y. Lee, and T. Nishino, Phys. Rev. A **83**, 052118 (2011).
[35] C. Hotta and N. Shibata, Phys. Rev. B **86**, 041108(R) (2012).
[36] C. Hotta, S. Nishimoto, and N. Shibata, Phys. Rev. B **87**, 115128 (2013).
[37] W. Yang, A. Nocera, and I. Affleck, Phys. Rev. Res. **2**, 033268 (2020).
[38] Γ terms usually work as an external field to have nematic order parameter, so that this state may seem natural. However, at $\theta = \pi/2$, the nematic phase does not happen even though $\Gamma = 1$ and $J = 0$, where we find a translational ferromagnetic phase. In the nematic singlet, the translational symmetry breaks as an interplay of frustration of both J and Γ.
[39] S. Sachdev and R. N. Bhatt, Phys. Rev. B **41**, 9323 (1990).
[40] H. T. Ueda and K. Totsuka, Phys. Rev. B **76**, 214428 (2007).
[41] See Supplemental Material at http://link.aps.org/supplemental/10.1103/PhysRevLett.132.166701 for the low energy excitations around the multicritical point, details of the entanglement property in Fig. 3(d), and the MPS solutions on a few other frustration-free models.
[42] B. S. Shastry and B. Sutherland, Phys. Rev. Lett. **47**, 964 (1981).
[43] M. Fannes, B. Nachtergaele, and R. F. Werner, Commun. Math. Phys. **144**, 443 (1992).
[44] U. Schollwöck, Ann. Phys. (Amsterdam) **326**, 96 (2011).
[45] S. Bravyi, L. Caha, R. Movassagh, D. Nagaj, and P. W. Shor, Phys. Rev. Lett. **109**, 207202 (2012).
[46] O. Salberger and V. Korepin, Rev. Math. Phys. **29**, 1750031 (2017).
[47] I. Lesanovsky, Phys. Rev. Lett. **108**, 105301 (2012).
[48] M. Fishman, S. White, and E. Stoudenmire, SciPost Phys. Codebases (2022), 10.21468/scipostphyscodeb.4.
[49] G. Vidal, J. I. Latorre, E. Rico, and A. Kitaev, Phys. Rev. Lett. **90**, 227902 (2003).
[50] P. Calabrese and J. Cardy, J. Stat. Mech. (2004) P06002.
[51] D. N. Sheng, O. I. Motrunich, and M. P. A. Fisher, Phys. Rev. B **79**, 205112 (2009).
[52] S. Friedemann, W. J. Duncan, M. Hirschberger, T. W. Bauer, R. Küchler, A. Neubauer, M. Brando, C. Pfleiderer, and F. M. Grosche, Nat. Phys. **14**, 62 (2018).
[53] Y. Ohmagari, T. Onimaru, Y. Yamane, Y. Shimura, K. Umeo, T. Takabatake, H. Sato, N. Kikugawa, T. Terashima, H. T. Hirose, and S. Uji, J. Phys. Soc. Jpn. **89**, 093701 (2020).
[54] F. Hori, K. Kinjo, S. Kitagawa, K. Ishida, Y. Ohmagari, and T. Onimaru, J. Phys. Conf. Ser. **2164**, 012027 (2022).
[55] F. Hori, K. Kinjo, S. Kitagawa, K. Ishida, S. Mizutani, R. Yamamoto, Y. Ohmagari, and T. Onimaru, Commun. Mater. **4**, 55 (2023).
[56] I. Affleck, T. Kennedy, E. H. Lieb, and H. Tasaki, Phys. Rev. Lett. **59**, 799 (1987).
[57] W. Dür, G. Vidal, and J. I. Cirac, Phys. Rev. A **62**, 062314 (2000).
[58] P. Klimov, R. Sengupta, and J. Biamonte, arXiv:2306.16456.
[59] D. M. Greenberger, M. A. Horne, and A. Zeilinger, Going beyond Bell's theorem, in *Bell's Theorem, Quantum Theory, and Conceptions of the Universe*, edited by M. Kafatos (Kluwer, Dordrecht, 1989), pp. 69–72.
[60] C. M. Caves, C. A. Fuchs, and R. Schack, J. Math. Phys. (N.Y.) **43**, 4537 (2002).
[61] R. N. Alexander, G. Evenbly, and I. Klich, Quantum **5**, 546 (2021).
[62] O. Salberger, T. Udagawa, Z. Zhang, H. Katsura, I. Klich, and V. Korepin, J. Stat. Mech. (2017) 063103.
[63] D. K. Mark, C.-J. Lin, and O. I. Motrunich, Phys. Rev. B **101**, 094308 (2020).